

Alkali doping of $\text{Zn}_x\text{Mg}_{1-x}\text{O}$ alloys for p -type conductivity

John L. Lyons*

Center for Computational Materials Science, US Naval Research Laboratory, Washington, D.C. 20375, USA

(Dated: July 17, 2025)

Nearly all ultrawide-bandgap oxides are affected by hole localization that limits p -type conductivity and thus potential applications for these materials. Highly localized holes, also known as hole polarons, trap in the vicinity of acceptor dopants, giving rise to large ionization energies and severely constraining free hole concentrations. Though this hole-trapping behavior affects wurtzite zinc oxide, rocksalt zinc oxide was recently found to be resistant to the formation of hole polarons. Moreover, p -type doping using lithium acceptors was predicted to be achievable. While rocksalt zinc oxide is metastable and has a band gap near ~ 3 eV, here it is found that zinc magnesium oxide ($\text{Zn}_x\text{Mg}_{1-x}\text{O}$) alloys remain p -type dopable within the stable rocksalt crystal structure, in addition to exhibiting band gaps in excess of 4 eV. As in rocksalt zinc oxide, alkali acceptors are shallow in zinc magnesium oxide and do not appear to be affected by donor compensation. These results indicate that alkali-doped $\text{Zn}_x\text{Mg}_{1-x}\text{O}$ alloys are a promising system for achieving a p -type dopable ultrawide-bandgap oxide.

I. INTRODUCTION

Ultrawide-bandgap (UWBG) semiconductors are of vital concern for future power and radio frequency electronics, ultraviolet light emitters, and semiconductor devices for extreme environments [1]. Nearly all of the UWBG materials exhibit unipolar electrical conductivity, where either only p -type (holes) or n -type (electrons) conductivity is possible, but not both. Since devices such as bipolar junction transistors and laser diodes usually require both kinds of conductivity, this shortcoming limits the applications of existing UWBG semiconductors.

In most materials, the major difficulty has been achieving reliable p -type conductivity.[1–4] (Diamond is an outlier, in that while modest p -type conductivity can be achieved,[5] n -type conductivity cannot.) AlN and AlGaIn have long been known to exhibit difficulties with p -type doping and exhibit very low doping efficiencies.[6, 7] Though c-BN has shown promise[8, 9] for acceptor doping (as well as for donor doping[10, 11]), reports are still limited, and growth of c-BN is difficult.

Oxides, and monoclinic gallium oxide ($\beta\text{-Ga}_2\text{O}_3$) in particular, have received significant attention as UWBG semiconductors.[1, 12, 13] However, holes have a tendency to strongly self trap in this class of materials.[4, 14, 15] These self-trapped holes (or hole polarons) strongly bind to acceptor dopants and give rise to large acceptor ionization energies.[16, 17] Recent theoretical studies indicate that rutile germanium oxide (r-GeO_2)[18] and rutile silicon dioxide (r-SiO_2)[19] might be less susceptible to hole localization, potentially enabling p -type conductivity in the rutile oxide materials family. However, methods to synthesize r-GeO_2 are still in their infancy,[20–22] and r-SiO_2 is a highly metastable phase[23] which will impair growth efforts. Other UWBG oxides have been proposed to potentially exhibit p -type

conductivity, such as LiGa_5O_8 , [24] but calculations indicate this material is also susceptible to hole localization and deep acceptor behavior.[25, 26]

Rocksalt oxides are a much less touted materials system among UWBG semiconductors, in comparison to $\beta\text{-Ga}_2\text{O}_3$ or r-GeO_2 . Much less is known about the behavior of defects and dopants in these systems, despite the prevalence of applications for MgO.[27] While dopants such as Li have experimentally been shown to be relatively deep acceptors in MgO[28], the reported ionization energies (near 0.7 eV) are smaller than other UWBG oxides such as Ga_2O_3 . Intriguingly, Goyal and Stevanović used hybrid functional calculations to show[29] that rocksalt zinc oxide (rs-ZnO), a metastable polymorph, was p -type dopable. Though the more stable wurtzite zinc oxide (wz-ZnO) also suffers from hole trapping and deep acceptor dopants[30], rs-ZnO has a higher valence-band edge and lower hole effective mass than wz-ZnO , both of which destabilize hole localization.

Though growth of rs-ZnO is likely difficult[31], rocksalt is the most stable crystal structure of magnesium oxide. A wide range of $\text{rs-Zn}_x\text{Mg}_{1-x}\text{O}$ alloys have been grown via pulsed laser deposition[32] or molecular beam epitaxy.[33, 34] Moreover, such alloys might be expected to exhibit the high densities that are thought to promote hole delocalization in UWBG oxides.[2, 3] Taken together, these results suggest that $\text{rs-Zn}_x\text{Mg}_{1-x}\text{O}$ might represent a readily synthesizable, p -type dopable UWBG oxide.

In this study, this possibility is explored using hybrid density functional theory. In agreement with prior experiments, alkali acceptors in rs-MgO are found to have high ionization energies, as they are affected by hole localization. However, calculations of the electronic structure of $\text{Zn}_x\text{Mg}_{1-x}\text{O}$ alloys indicate that they share similar properties to rs-ZnO . Explicit defect modeling in the $\text{Zn}_x\text{Mg}_{1-x}\text{O}$ alloys (for both ordered and disordered structures) show that alkali acceptors are shallow dopants in these alloys, and that under O-rich conditions compensation of p -type doping can be avoided.

* john.l.lyons27.civ@us.navy.mil

material	bandgap (eV)		a (Å)	
	calc.	exp.	calc.	exp.
rs-ZnO	3.57 (<i>i</i>)	2.75[42]	4.24	4.27[43]
rs-Zn _{0.5} Mg _{0.5} O	4.41 (<i>i</i>)	—	4.20	—
rs-MgO	7.55 (<i>d</i>)	7.78[39]	4.16	4.22[40]

TABLE I. Structure and electronic properties of ZnO, MgO, and the ordered Zn_{0.5}Mg_{0.5}O alloy in the rocksalt crystal structure. Band gaps are listed in eV, and lattice parameters are in Å. ZnO and Zn_{0.5}Mg_{0.5}O have indirect (*i*) bandgaps, while MgO has a direct (*d*) bandgap at Γ ; full band structures are provided in Appendix A.

II. METHODS

To calculate defects and dopants in MgO and Zn_xMg_{1-x}O alloys, hybrid DFT calculations are employed using the projector-augmented wave method [35] implemented in VASP [36], and with a 400 eV planewave cutoff. $8 \times 8 \times 8$ Γ -centered k -point meshes were used to optimize the lattice parameters of primitive cells of rs-ZnO and rs-MgO, and $6 \times 6 \times 6$ Γ -centered k -point meshes were used to optimize the lattice parameters of 8-atom cells of ordered Zn_xMg_{1-x}O alloys.

The HSE hybrid functional [37, 38] with 34.5% mixing and a screening parameter of 0.2 \AA^{-1} is used for all compounds in this work. This provides an excellent description of the band gap[39] and lattice parameters[40] for MgO, which are in good agreement with experimentally observed values and prior theoretical work[27, 41]. The HSE-calculated structural and electronic properties of ZnO, MgO, and the ordered Zn_{0.5}Mg_{0.5}O alloy, all in the rocksalt crystal structure, are listed in Table 1.

For defect calculations, 216-atom supercells with one k -point at Γ are used for both MgO and the ordered-alloy calculations. (For the random alloy structures, which are discussed in Appendix B, 64-atom rocksalt supercells are used.) The formalism established in Ref. 44 is used to calculate defect formation energies. Taking the example of the lithium substitutional acceptor in MgO (Li_{Mg}) as an example, its formation energy in charge state q is given by:

$$E^f(\text{Li}_{\text{Mg}}^q) = E_{\text{tot}}(\text{Li}_{\text{Mg}}^q) - E_{\text{tot}}(\text{MgO}) + \mu_{\text{Mg}} - \mu_{\text{Li}} + q(\varepsilon_F + \varepsilon_v) + \Delta^q, \quad (1)$$

where $E_{\text{tot}}(\text{Li}_{\text{Mg}}^q)$ is the total energy of a supercell containing the Li acceptor in charge state q , and $E_{\text{tot}}(\text{MgO})$ is the total energy of pristine MgO using the same supercell. Any electrons added to or removed from the supercell are exchanged with the electron reservoir in the semiconductor host, i.e., the Fermi level (ε_F), which is referenced to the VBM of MgO (ε_v). The final term in Eq. 1, Δ^q , is the charge-state dependent term that corrects for the finite size of the charged supercell [45, 46].

The removed Mg atom is placed in a reservoir of energy μ_{Mg} , referenced to the energy per atom of Mg metal. The range of μ_{Mg} is limited by the enthalpy of formation of

MgO [$\Delta H_f(\text{MgO})$, calculated to be -5.80 eV], so μ_{Mg} can take values between 0 eV (the Mg-rich limit) and -5.80 eV (the O-rich limit). Analogous considerations apply to μ_{O} , which is referenced to one half of the energy of the spin-polarized O₂ molecule.

The chemical potential for the impurity is limited by the formation of secondary phases; in the case of Li, μ_{Li} is limited by the formation of Li₂O through the relation:

$$2\mu_{\text{Li}} + \mu_{\text{O}} < \Delta H_f(\text{Li}_2\text{O}), \quad (2)$$

where $\Delta H_f(\text{Li}_2\text{O})$ is the formation enthalpy of Li₂O [calculated to be -5.85 eV]. Analogous expressions can be written for the secondary phases that limit the chemical potentials of other impurities (e.g., Na₂O for Na and K₂O for K).

Band alignments between the binary compounds and Zn_xMg_{1-x}O ordered alloys are calculated using surface-slab calculations, which align the VBM of each oxide (referenced to the averaged electrostatic potential within each compound) to the vacuum level. This approach provides a common reference and avoids strain effects [47]. Nonpolar (100) surfaces are used for these calculations, with eight bilayers of oxide (at least 15 \AA of material) together with 25 \AA of vacuum. Atoms within 5 \AA of each surface were relaxed, while interior atoms had positions fixed in order to mimic bulk material.

III. RESULTS AND DISCUSSION

A. Bulk properties of rocksalt ZnO, Zn_{0.5}Mg_{0.5}O, and MgO

The HSE-calculated band gaps and lattice parameters for rocksalt MgO, ZnO, and Zn_{0.5}Mg_{0.5}O are compared in Table I against the available experimental values. Both the calculated lattice parameter (4.16 \AA) and band gap (7.55 eV) of MgO are in good agreement with experiments, which yielded values of 4.22 \AA [40] and 7.78 eV [39]. The calculated lattice parameter of rs-ZnO (4.24 \AA) is also in good agreement with the experimental value (4.27 \AA)[43]. The lattice parameter of Zn_{0.5}Mg_{0.5}O falls halfway between MgO and ZnO, as would be expected by Vegard's law.

While the calculated band gap of rs-ZnO (3.57 eV) is larger than the reported experimental gap of 2.75 eV [42], reports on this material are limited. Moreover, due to its metastability, crystal quality might limit reliability. It should also be noted that the higher gap reported here is more consistent with prior theoretical reports[3, 29], and that similarly high mixing parameters are needed to accurately describe the electronic structure of wz-ZnO.[30]

In agreement with previous work,[41] MgO has a direct band gap at Γ ; while the indirect gap of rs-ZnO (with the VBM at L and the conduction-band minimum at Γ) also agrees with the results from Ref. 29. The band gap of ordered Zn_{0.5}Mg_{0.5}O (which is also indirect) deviates from Vegard's law, but is consistent with the band-gap

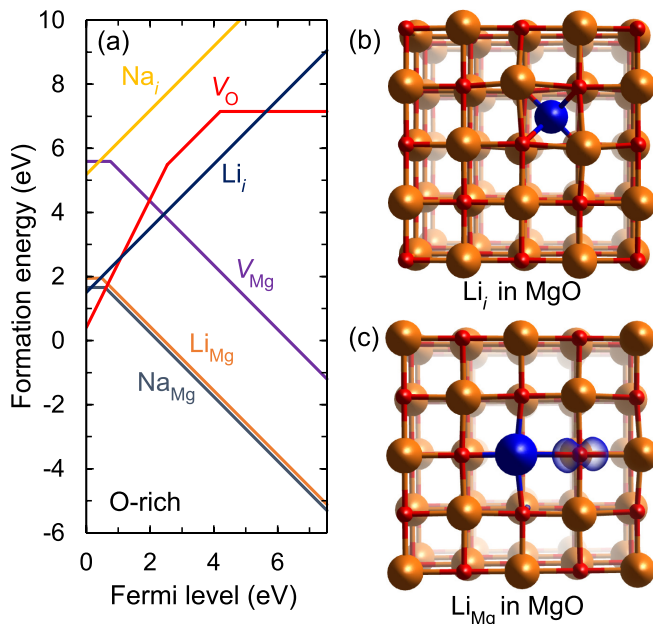


FIG. 1. (a) Formation energy versus Fermi level for impurities and defects in MgO under O-rich conditions. (b) Structure of the Li_i donor in MgO, with Mg atoms in orange, O atoms in red, and Li in blue. (c) Isosurface (in blue) of the spin density for the Li_Mg acceptor in MgO. (Plotted using VESTA[48]).

bowing that has previously been observed[34] in this alloy system. HSE-calculated band structures are included in Fig. 4 of Appendix A.

B. Doping of rocksalt MgO

In Fig. 1 the results for alkali doping of rs-MgO are summarized, showing that Li and Na can incorporate as acceptors on the Mg site. Unlike in rs-ZnO, alkali substitutionals can trap hole polarons in rs-MgO and exhibit deep transition levels. As shown in Fig. 1c, these holes trap onto an oxygen site that is a nearest neighbor to the substitutional impurity. This hole localization results in large acceptor ionization energies: the smallest occurs for Na_Mg (0.49 eV), while those of Li_Mg (0.59 eV) and K_Mg (0.76 eV) are larger. The calculated transition level of Li_Mg (0.59 eV) is similar to a prior experimental report[28] of a 0.7 eV activation energy measured in Li-doped MgO.

These results indicate that rs-MgO will itself not be highly *p*-type dopable with alkali elements, as the large ionization energies will limit the number of free hole concentrations that can arise from acceptor doping. Still, the ionization energies calculated here for rs-MgO are only slightly larger than those of GeO_2 [18], and are smaller than many other UWBG oxides[15–17].

The formation energies of possible compensating species, including oxygen vacancies (V_O) and alkali donor

interstitials (including Na_i and Li_i), are also shown in Fig. 1. The O-rich extreme is considered; as discussed in Ref. 29, these conditions are most favorable for the incorporation of the alkali substitutional acceptors. For most Fermi levels, Li_Mg and Na_Mg acceptors (which have nearly the same formation energy) are the lowest-energy defects among those considered. Compensating self interstitials (e.g., Na_i and Li_i) are much higher in energy over most of the band gap; only when ε_F nears 0 eV (i.e., *p*-type conditions) does the formation energy of Li_i approach that of Li_Mg . In contrast, Na_i is 3 eV higher in energy than Na_Mg , even when $\varepsilon_F = 0$ eV.

These results suggest that, like in rs-ZnO, alkali acceptor dopants in MgO can avoid being compensated by native defects or alkali interstitial donors. Thus, if the ionization energies of the acceptor dopants could somehow be lowered, *p*-type conductivity could be achieved in this material family. Because alkali acceptors in rs-ZnO have been previously found to exhibit small ionization energies, this suggests that $\text{Zn}_x\text{Mg}_{1-x}\text{O}$ alloys might be a viable system for achieving *p*-type conductivity. Before exploring this possibility, the role of Zn alloying on the rs-MgO electronic structure is first considered.

C. Electronic structure of ordered $\text{Zn}_x\text{Mg}_{1-x}\text{O}$ alloys

Incorporating Mg into rs-ZnO increases the band gap of the $\text{Zn}_x\text{Mg}_{1-x}\text{O}$ alloy, but it does not substantively affect other aspects of the band structure, as shown in Fig. 4b-d of Appendix A. The VBM remains at the L point for the intermediate alloys, as the relative energy of the conduction-band minimum (CBM) at Γ moves upward. This yields indirect bandgaps of 3.88 eV for $\text{Zn}_{0.75}\text{Mg}_{0.25}\text{O}$, 4.40 eV for $\text{Zn}_{0.5}\text{Mg}_{0.5}\text{O}$, and 5.16 eV for $\text{Zn}_{0.25}\text{Mg}_{0.75}\text{O}$.

Note that these values are for the case of ordered alloys. For the random alloy, $\text{Zn}_{0.5}\text{Mg}_{0.5}\text{O}$ is calculated to have a band gap only 0.16 eV larger (4.56 eV), suggesting that disorder does not have a major effect on the band structure of the oxide. It should also be noted that disorder does not strongly affect the energetics of the $\text{Zn}_x\text{Mg}_{1-x}\text{O}$ alloy, as the disordered compound is within 0.01 eV/formula unit of the ordered structure for $\text{Zn}_{0.5}\text{Mg}_{0.5}\text{O}$.

The trends in the electronic structure can be seen in Fig. 2. As shown in Fig. 2a, the band gap remains indirect in rs-ZnO and in the $\text{Zn}_x\text{Mg}_{1-x}\text{O}$ alloys. Both the direct and indirect gaps increase rapidly as Mg content increases. In MgO, the valence band at the L point moves below the VBM at Γ , leaving a large direct gap (as shown in Appendix A).

In Fig. 2b the absolute trends in energies of the bands can be observed for the ordered alloys. (As discussed in the Methods section, these energies are referenced to the vacuum level via surface-slab calculations.) These results show that as the Mg content in the $\text{Zn}_x\text{Mg}_{1-x}\text{O}$ alloy is

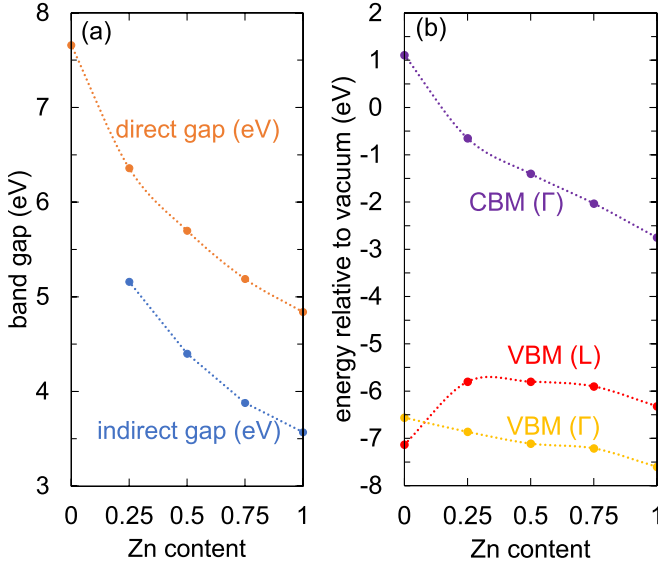


FIG. 2. (a) Direct and indirect band gaps as a function of Zn content in $\text{Zn}_x\text{Mg}_{1-x}\text{O}$ alloys. (b) Energies (in eV, with respect to vacuum) for the different high-symmetry points in the band structures of $\text{Zn}_x\text{Mg}_{1-x}\text{O}$ alloys. Dotted lines are guides for the eye.

increased, the L-point VBM rises slightly in energy, while the CBM (at Γ) increases rapidly with Mg content. Only once Zn is no longer present (i.e., for pure MgO) does the VBM revert to the Γ point, yielding the large direct gap of MgO. These results suggest that the electronic structure of $\text{rs-Zn}_x\text{Mg}_{1-x}\text{O}$ alloys will be similar to that of rs-ZnO , with the valence-band properties being driven by the maximum at the L point (albeit with a larger band gap). Thus, if the ionization energies in the alloy are similar to rs-ZnO , p -type dopability should also be achieved.

D. Doping of rocksalt $\text{Zn}_{0.5}\text{Mg}_{0.5}\text{O}$

The behavior of alkali impurities in $\text{Zn}_{0.5}\text{Mg}_{0.5}\text{O}$ is found to be similar to what was reported previously in Ref. 29 for rs-ZnO . In Fig. 3, the formation energy (in eV) versus Fermi level (also in eV) is plotted for alkali substitutional acceptors and compared with native defects and alkali interstitials. (Though these calculations used an ordered $\text{Zn}_{0.5}\text{Mg}_{0.5}\text{O}$ supercell, the results presented in Appendix B indicate that disorder will not strongly affect the conclusions.) As with rs-ZnO , [29] the alkali substitutional acceptors are shallow, and do not exhibit deep transition levels. This behavior is attributed to the high-lying L-point VBM, which suppresses hole polaron formation, as was also reported for rs-ZnO . Both Li and Na substitutional acceptors are found to act as effective-mass acceptors, with ionization energies near ~ 0.1 - 0.2 eV.

The energy of the Li and Na cation-site substitutional

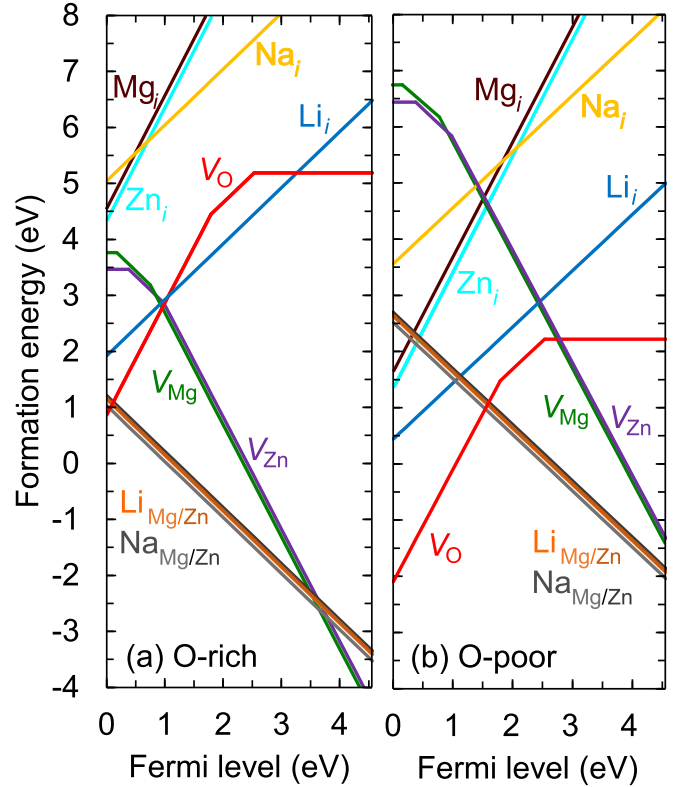


FIG. 3. Formation energy versus Fermi level for impurities and defects in $\text{Zn}_{0.5}\text{Mg}_{0.5}\text{O}$ under (a) O-rich and (b) O-poor conditions. The formation energies of the alkali substitutional acceptor dopants (Li_{Zn} in dark orange, Li_{Mg} in light orange, Na_{Zn} in light gray, and Na_{Mg} in dark grey) are clustered at similar energies in both cases.

acceptors are quite similar, regardless of which site onto which they incorporate. As seen in Fig. 3, the formation energies of Li_{Zn} , Li_{Mg} , Na_{Zn} , and Na_{Mg} cluster within about 0.2 eV. This can be attributed to the fact that both Zn and Mg are surrounded only by O nearest neighbors in the $\text{Zn}_x\text{Mg}_{1-x}\text{O}$ alloy; since defect properties are driven mainly by nearest neighbors, it follows that cation-site substitutionals from similar impurities will lead to similar properties. (Similar conclusions were reached in a prior study of substitutional dopants in InGaN alloys.[49]) Choice of cation site also minimally affects the structural properties: Na_{Zn} features Na–O average bond lengths of 2.18 Å versus 2.21 Å for Na_{Mg} , while Li_{Zn} has Li–O bond lengths of 2.12 Å versus 2.16 Å for Li_{Mg} . This behavior is not likely to extend to the larger alkali elements, however: potassium substituting for Zn or Mg in ordered $\text{Zn}_{0.5}\text{Mg}_{0.5}\text{O}$ leads to polaronic acceptor behavior, with ionization energies near 0.3 eV.

Competition with native acceptors will not apparently affect the incorporation of alkali dopants. Under n -type conditions (e.g., when the Fermi level is near the CBM), the cation vacancies (V_{Zn} and V_{Mg}) have lower formation energies than the alkali substitutional acceptors under O-rich conditions. However, as the Fermi level moves

towards the VBM (e.g., under p -type conditions), the alkali substitutionals become lower in energy.

Compensation by donors also appears to be avoidable under the O-rich conditions shown in Fig. 3a. Both alkali interstitial donors are significantly higher in energy than the alkali substitutional acceptors, especially under O-rich conditions, and neither should be a source of compensation in alkali-doped material. Only when the Fermi level is at the VBM does the formation of V_O approach that of the acceptor dopants, suggesting that these species will also not be a source of compensation under O-rich conditions. Native interstitial donors (e.g., Zn_i and Mg_i) have higher formation energies than Li_i under all conditions.

Based on these results, sodium seems to be the best candidate for acceptor doping of $Zn_{0.5}Mg_{0.5}O$, since its donor interstitial is high in energy and does not appear to be a potential compensating species. Oxygen vacancies do appear to be the most likely compensating donors, but their presence could be minimized with growth under the O-rich extreme. Prior work[28] on Li doping of MgO suggested that oxidation of doped crystals was important for electrically activating the acceptor; similar approaches might also be explored for the $Zn_xMg_{1-x}O$ alloys.

IV. SUMMARY AND CONCLUSIONS

Using hybrid density functional calculations, the electronic structures of $Zn_xMg_{1-x}O$ alloys were calculated, and the behavior of alkali dopants was determined in both rocksalt MgO and $Zn_{0.5}Mg_{0.5}O$. Like rocksalt ZnO, the $Zn_xMg_{1-x}O$ alloys exhibit indirect band gaps, with the valence-band maxima occurring away from the Γ point. This higher-lying band promotes hole delocalization, and leads to shallow acceptor behavior for Li and Na substitutional acceptors. Moreover, acceptor doping should be free from compensation, at least towards O-rich conditions, as these acceptor impurities have formation energies lower than potential compensating donors such as oxygen vacancies and alkali interstitials. As the synthesis of rocksalt $Zn_xMg_{1-x}O$ alloys has already proven feasible, this study indicates that these materials are a promising direction for p -type-dopable ultrawide-bandgap oxides.

V. ACKNOWLEDGEMENTS

This work was supported by the Office of Naval Research through the Naval Research Laboratory's Base Research Program. Computations were performed at the DoD Major Shared Resource Centers at AFRL and the Army ERDC. Henryk Teisseyre is thanked for illuminating discussions.

VI. DATA AVAILABILITY

The data the support the findings of this study are available upon request.

VII. APPENDIX A: BAND STRUCTURES OF COMPOUNDS

The band structures of ZnO, MgO, and ordered $Zn_xMg_{1-x}O$ alloys, all in the rocksalt crystal structure, are shown in Fig. 4. All calculations utilize the self-consistent HSE hybrid functional, with 34.5% exact exchange and a screening parameter of 0.2 \AA^{-1} . As in prior studies [29, 50], it is found that rs-ZnO has an indirect band gap, with the VBM located at the L point and the CBM located at the Γ point. The calculated rs-ZnO band gap is 3.57 eV, as shown in Table I. Due to the use of a higher mixing parameter, the calculated band gap is larger than in prior studies, as discussed in the main text.

Consistent with prior reports,[41] rs-MgO has a direct band gap at Γ , along with a much larger band gap (7.55 eV) than rs-ZnO. The calculated band gap of rs-MgO is close to the experimental band gap of 7.78 eV[39], and is similar to results from *GW* calculations.[27]

As Mg increases in the $Zn_xMg_{1-x}O$ alloy, the band gaps steadily increase, with noticeable downward band bowing. This behavior is consistent with prior studies,[34] though the calculated band gaps fall at the lower end of the reported values. This may be due in part to the use of ordered alloys in this work: the disordered alloy of $Zn_{0.5}Mg_{0.5}O$ is calculated here to have a band gap 0.15 eV larger than the ordered structure.

For all cases, the VBM is set to 0 eV (i.e., the band structures are not aligned to a common reference). However, Fig. 2b in the main text displays how band-edge energies change as a function of energy.

VIII. APPENDIX B: DEFECT FORMATION ENERGIES IN RANDOM ALLOYS

The formation energies of defects and dopants versus the Fermi level are shown in Fig. 5 for the case of rs- $Zn_{0.5}Mg_{0.5}O$ in a disordered 64-atom supercell. For these calculations, six different configurations for each defect are selected (at distinct sites in the supercell), and formation energies are averaged over the resulting formation energies. Solid lines in the figure indicate the average of these formation energies, while the color-coded dotted lines indicate the standard deviation of formation energies.

In agreement with the results discussed in Fig. 3 of the main text, there is little variability among the cation-site substitutional acceptors (i.e., Na_{Zn} , Na_{Mg} , Li_{Zn} , and Li_{Mg}). Again, this can be attributed to the fact that

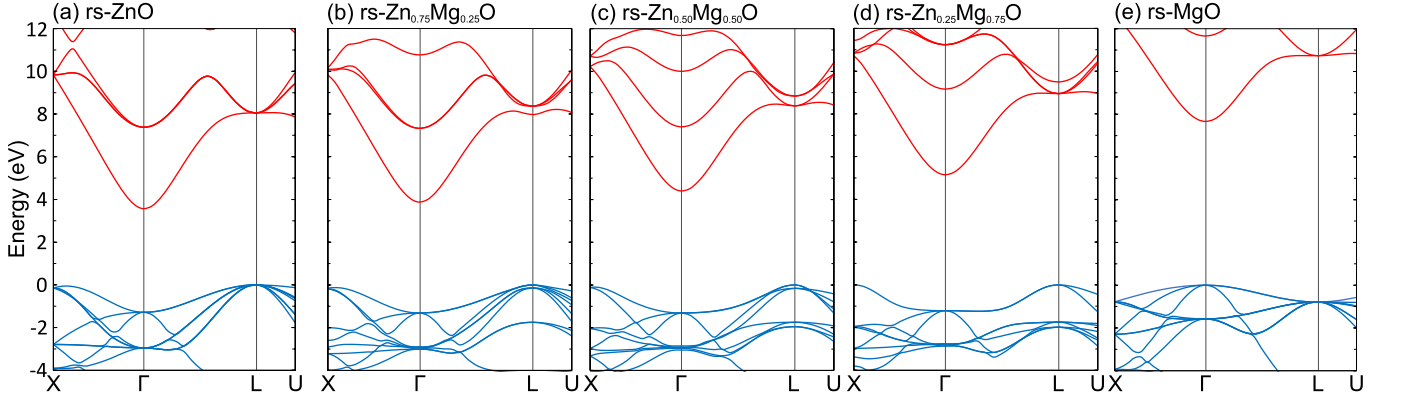


FIG. 4. HSE-calculated band structures of (a) rs-ZnO, (b) rs-Zn_{0.75}Mg_{0.25}O, (c) rs-Zn_{0.5}Mg_{0.5}O, (d) rs-Zn_{0.25}Mg_{0.75}O, and (e) rs-MgO. Valence bands are drawn in blue, while conduction bands are drawn in red, and the VBM is set to 0 eV for each system.

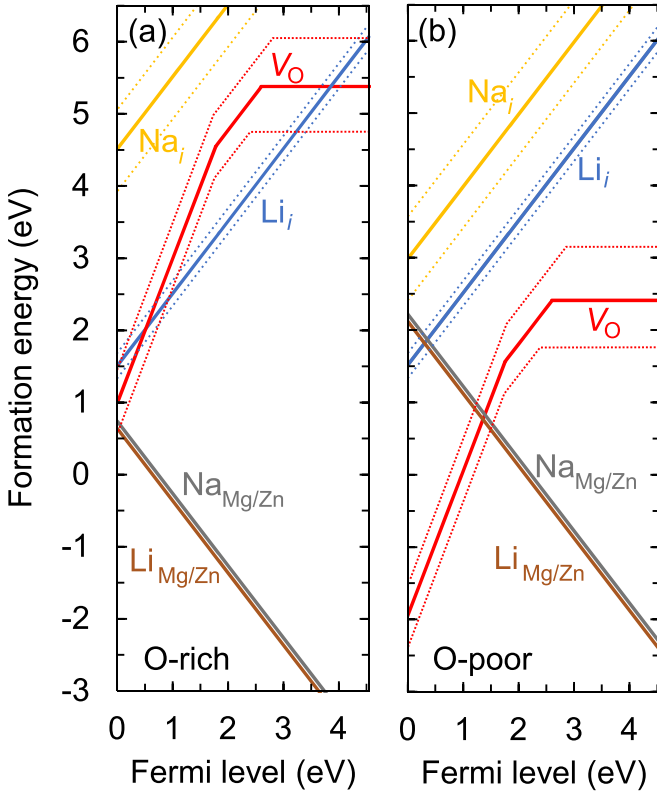


FIG. 5. Formation energy versus Fermi level for impurities and defects in rs-Zn_{0.5}Mg_{0.5}O under (a) O-rich and (b) O-poor conditions. Solid lines represent the formation energies averaged over all configurations, while dotted lines represent a standard deviation on each side of the average.

these acceptors have only oxygen atoms as nearest neighbors. Thus their character, which is mainly driven by nearest neighbors,[49] is not strongly impacted by Zn/Mg disorder. In agreement with the ordered-cell calculations, acceptor dopants in the disordered cell are most stable under O-rich conditions, where they do not appear to be strongly affected by compensating donors (such as V_O and Li_i/Na_i). All acceptor dopants also act as shallow acceptors, in agreement with the ordered-supercell calculations.

Larger variability is observed for the formation energies of the compensating donors Na_i , Li_i , and V_O . The range of formation energies is largest for V_O^0 (nearly 1.5 eV) and for Na_i (1.2 eV). Unlike the substitutional alkali acceptors, these species can be affected by alloy disorder, because their nearest neighbors are not necessarily cations.

Nevertheless, the conclusions that can be drawn from the disordered-supercell results of Fig. 5 are similar to those from Fig. 3 in the main text. Namely, that acceptor doping should be most effective under O-rich conditions, where the alkali interstitials (Na_i and Li_i) are high in energy, and that V_O only compete with the dopants when the Fermi level is near the VBM. As was the case for the ordered-supercell calculations, the formation energies of the acceptor dopants are higher in O-poor conditions, where V_O becomes the dominant defect when the Fermi level moves to within 1.5 eV of the VBM.

IX. REFERENCES

[1] J. Y. Tsao, S. Chowdhury, M. A. Hollis, D. Jena, N. M. Johnson, K. A. Jones, R. J. Kaplar, S. Rajan, C. G. Van de Walle, E. Bellotti, C. L. Chua, R. Collazo, M. E.

Coltrin, J. A. Cooper, K. R. Evans, S. Graham, T. A. Grotjohn, E. R. Heller, M. Higashiwaki, M. S. Islam, P. W. Juodawlkis, M. A. Khan, A. D. Koehler, J. H.

- Leach, U. K. Mishra, R. J. Nemanich, R. C. N. Pilawa-Podgurski, J. B. Shealy, Z. Sitar, M. J. Tadjar, A. F. Witulski, M. Wraback, and J. A. Simmons, "Ultrawide-bandgap semiconductors: Research opportunities and challenges," *Adv. Elec. Mat.* **4**, 1600501 (2017).
- [2] J. L. Lyons, D. Wickramaratne, and A. Janotti, "Dopants and defects in ultra-wide bandgap semiconductors," *Current Opinion in Solid State and Materials Science* **30**, 101148 (2024).
- [3] S. Chae, N. Sanders, K. A. Mengle, A. Wang, X. Zhang, J. L. Bartolome, K. Luo, Y.-C. Huang, F. Giustino, J. T. Heron, and E. Kioupakis, "Extreme-band-gap semiconductors with shallow dopants and mobile carriers," (2025), [arXiv:2506.07284 \[cond-mat.mtrl-sci\]](#).
- [4] T. N. H. Vu and Y. Kumagai, "Can the oxygen 2p band be hole doped?" (2025), [arXiv:2506.11619 \[cond-mat.mtrl-sci\]](#).
- [5] E. Visser, G. Bauhuis, G. Janssen, W. Vollenberg, J. Willem, W. van Enkevort, and L. Giling, "Electrical conduction in homoepitaxial, boron-doped diamond films," *J. Phys.: Condens. Matter* **4**, 7365–7376 (1992).
- [6] Y. Taniyasu, M. Kasu, and T. Makimoto, "An aluminium nitride light-emitting diode with a wavelength of 210 nanometres," *Nature* **441**, 325–328 (2006).
- [7] T. Kolbe, A. Knauer, J. Rass, H. K. Cho, S. Hagedorn, F. Bilchenko, A. Muhi, J. Ruschel, M. Kneissl, S. Einfeldt, and M. Weyers, "234 nm far-ultraviolet-C light-emitting diodes with polarization-doped hole injection layer," *Appl. Phys. Lett.* **122**, 191101 (2023).
- [8] O. Mishima, J. Tanaka, S. Yamaoka, and O. Fukunaga, "High-temperature cubic boron nitride p-n junction diode made at high pressure," *Science* **238**, 181 (1987).
- [9] L. Weston, D. Wickramaratne, and C. G. Van de Walle, "Hole polarons and p-type doping in boron nitride polymorphs," *Phys. Rev. B* **96**, 100102R (2017).
- [10] K. Hiram, Y. Taniyasu, H. Yamamoto, and K. Kumamura, "Control of n-type electrical conductivity for cubic boron nitride (c-BN) epitaxial layers by Si doping," *Appl. Phys. Lett.* **116**, 162104 (2020).
- [11] M. E. Turiansky, D. Wickramaratne, J. L. Lyons, and C. G. Van de Walle, "Prospects for n-type conductivity in cubic boron nitride," *Appl. Phys. Lett.* **119**, 162105 (2021).
- [12] M. Higashiwaki, K. Sasaki, H. Murakami, Y. Kumagai, A. Koukitu, A. Kuramata, T. Masui, and S. Yamakoshi, "Recent progress in Ga₂O₃ power devices," *Semiconductor Science and Technology* **31**, 034001 (2016).
- [13] M. J. Tadjar, J. L. Lyons, N. Nepal, J. A. Freitas, A. D. Koehler, and G. M. Foster, "Editors' choice—review—theory and characterization of doping and defects in β -Ga₂O₃," *ECS J. Sol. State Sci. Technol.* **8**, Q3187–Q3194 (2019).
- [14] J. B. Varley, A. Janotti, C. Franchini, and C. G. Van de Walle, "Role of self-trapping in luminescence and p-type conductivity of wide-band-gap oxides," *Phys. Rev. B* **85**, 081109 (2012).
- [15] J. L. Lyons, "Self-trapped holes and polaronic acceptors in ultrawide-bandgap oxides," *J. Appl. Phys.* **131**, 025701 (2022).
- [16] A. Kyrtos, M. Matsubara, and E. Bellotti, "On the feasibility of p-type Ga₂O₃," *Appl. Phys. Lett.* **112**, 032108 (2018).
- [17] J. L. Lyons, "A survey of acceptor dopants for β -Ga₂O₃," *Semicon. Sci. Technol.* **33**, 05LT02 (2018).
- [18] S. Chae, J. Lee, K. A. Mengle, J. T. Heron, and E. Kioupakis, "Rutile GeO₂: An ultrawide-band-gap semiconductor with ambipolar doping," *Appl. Phys. Lett.* **114**, 102104 (2019).
- [19] J. L. Lyons and A. Janotti, "A p-type dopable ultrawide-bandgap oxide," *J. Phys.: Cond. Matter* **36**, 085501 (2023).
- [20] C. A. Niedermeier, K. Ide, T. Katase, H. Hosono, and T. Kamiya, "Shallow valence band of rutile GeO₂ and p-type doping," *J. Phys. Chem. C* **124**, 25721–25728 (2020).
- [21] I. Rahaman, H. D. Ellis, K. Anderson, M. A. Scarpulla, and K. Fu, "Growth of GeO₂ on r-plane and c-plane sapphires by MOCVD," *ACS Applied Engineering Materials* **2**, 1724–1736 (2024).
- [22] Z. Galazka, R. Blukis, A. Fiedler, S. Bin Anooz, J. Zhang, M. Albrecht, T. Remmele, T. Schulz, D. Klimm, M. Pietsch, A. Kwasniewski, A. Dittmar, S. Ganschow, U. Juda, K. Stolze, M. Suendermann, T. Schroeder, and M. Bickermann, "Bulk single crystals and physical properties of rutile GeO₂ for high-power electronics and deep-ultraviolet optoelectronics," *physica status solidi (b)* **n/a**, 2400326 (2024).
- [23] N. M. K. Linn, M. Madal, B. Li, Y. Fei, and K. Landskron, "Insights into the hydrothermal metastability of stishovite and coesite," *ACS Omega* **3**, 14225 (2018).
- [24] K. Zhang, V. G. T. Vangipuram, H.-L. Huang, J. Hwang, and H. Zhao, "Discovery of a robust p-type ultrawide bandgap oxide semiconductor: LiGa₅O₈," *Advanced Electronic Materials* **11**, 2300550 (2025).
- [25] J. L. Lyons, "Deep polaronic acceptors in LiGa₅O₈," *J. Appl. Phys.* **135**, 165705 (2024).
- [26] K. Dabsamut, K. Takahashi, and W. R. L. Lambrecht, "Native defects and their complexes in spinel LiGa₅O₈," *J. Appl. Phys.* **135**, 235707 (2024).
- [27] P. Rinke, A. Schleife, E. Kioupakis, A. Janotti, C. Rödl, F. Bechstedt, M. Scheffler, and C. G. Van de Walle, "First-principles optical spectra for f centers in MgO," *Phys. Rev. Lett.* **108**, 126404 (2012).
- [28] M. M. Tardío, R. Ramírez, R. González, and Y. Chen, "p-type semiconducting properties in lithium-doped MgO single crystals," *Phys. Rev. B* **66**, 134202 (2002).
- [29] A. Goyal and V. Stevanović, "Metastable rocksalt ZnO is p-type dopable," *Phys. Rev. Mater.* **2**, 084603 (2018).
- [30] J. L. Lyons, A. Janotti, and C. G. Van de Walle, "Why nitrogen cannot lead to p-type conductivity in ZnO," *Appl. Phys. Lett.* **95**, 252105 (2009).
- [31] F. Decremps, J. Pellicer-Porres, F. Datchi, J. P. Itié, A. Polian, F. Baudelet, and J. Z. Jiang, "Trapping of cubic ZnO nanocrystallites at ambient conditions," *Appl. Phys. Lett.* **81**, 4820–4822 (2002).
- [32] S. Choopun, R. D. Vispute, W. Yang, R. P. Sharma, T. Venkatesan, and H. Shen, "Realization of band gap above 5.0 eV in metastable cubic-phase Mg_xZn_{1-x}O alloy films," *Appl. Phys. Lett.* **80**, 1529–1531 (2002).
- [33] C.-Y. J. Lu, Y.-T. Tu, T. Yan, A. Trampert, L. Chang, and K. H. Ploog, "Growth and stability of rocksalt Zn_{1-x}Mg_xO epilayers and ZnO/MgO superlattice on MgO (100) substrate by molecular beam epitaxy," *J. Chem. Phys.* **144**, 214704 (2016).
- [34] I. Gorczyca, M. Wierzbowska, D. Jarosz, J. Z. Domagala, A. Reszka, D. Le Si Dang, F. Donatini, N. E. Christensen, and H. Teisseyre, "Rocksalt ZnMgO alloys for ultraviolet

- applications: Origin of band-gap fluctuations and direct-indirect transitions,” *Phys. Rev. B* **101**, 245202 (2020).
- [35] P. E. Blöchl, “Projector augmented-wave method,” *Phys. Rev. B* **50**, 17953 (1994).
- [36] G. Kresse and J. Joubert, “From ultrasoft pseudopotentials to the projector augmented-wave method,” *Phys. Rev. B* **59**, 1758 (1999).
- [37] J. Heyd, G. E. Scuseria, and M. Ernzerhof, “Hybrid functionals based on a screened Coulomb potential,” *J. Chem. Phys.* **118**, 8207 (2003).
- [38] J. Heyd, G. E. Scuseria, and M. Ernzerhof, “Erratum: ”Hybrid functionals based on a screened Coulomb potential” [J. Chem. Phys. 118, 8207 (2003)],” *J. Chem. Phys.* **124**, 219906 (2006).
- [39] R. C. Whited and W. C. Walker, “Exciton spectra of CaO and MgO,” *Phys. Rev. Lett.* **22**, 1428–1430 (1969).
- [40] K. Hirata, K. Moriya, and Y. Waseda, “High temperature thermal expansion of ThO₂, MgO, and Y₂O₃ by X-ray diffraction,” *Journal of Materials Science* **12**, 838–839 (1977).
- [41] A. Schleife, F. Fuchs, J. Furthmüller, and F. Bechstedt, “First-principles study of ground- and excited-state properties of MgO, ZnO, and CdO polymorphs,” *Phys. Rev. B* **73**, 245212 (2006).
- [42] J. A. Sans, A. Segura, F. J. Manjón, B. Marí, A. Muñoz, and M. J. Herrera-Cabrera, “Optical properties of wurtzite and rock-salt ZnO under pressure,” *Microelectronics Journal* **36**, 928–932 (2005).
- [43] H. Karzel, W. Potzel, M. Köfferlein, W. Schiessl, M. Steiner, U. Hiller, G. M. Kalvius, D. W. Mitchell, T. P. Das, P. Blaha, K. Schwarz, and M. P. Pasternak, “Lattice dynamics and hyperfine interactions in ZnO and ZnSe at high external pressures,” *Phys. Rev. B* **53**, 11425–11438 (1996).
- [44] C. Freysoldt, B. Grabowski, T. Hickel, J. Neugebauer, G. Kresse, A. Janotti, and C. G. Van de Walle, “First-principles calculations for point defects in solids,” *Rev. Mod. Phys.* **86**, 253–305 (2014).
- [45] C. Freysoldt, J. Neugebauer, and C. G. Van de Walle, “Fully *abinitio* finite-size corrections for charged-defect supercell calculations,” *Phys. Rev. Lett.* **102**, 016402 (2009).
- [46] C. Freysoldt, J. Neugebauer, and C. G. Van de Walle, “Electrostatic interactions between charged defects in supercells,” *Phys. Stat. Sol. B* **248**, 1067 (2011).
- [47] A. Franciosi and C. G. Van de Walle, “Heterostructure band offset engineering,” *Surf. Sci.* **25**, 1 (1996).
- [48] K. Momma and F. Izumi, “VESTA 3 for three-dimensional visualization of crystal, volumetric and morphology data,” *J. Appl. Crystallogr.* **44**, 1272–1276 (2011).
- [49] D. Wickramaratne, C. E. Dreyer, J.-X. Shen, J. L. Lyons, A. Alkauskas, and C. G. Van de Walle, “Deep-level defects and impurities in InGaN alloys,” *physica status solidi (b)* **257**, 1900534 (2020).
- [50] S. Lany, “Polymorphism, band-structure, band-lineup, and alloy energetics of the group II oxides and sulfides MgO, ZnO, CdO, MgS, ZnS, CdS,” in *Oxide-based Materials and Devices V*, Vol. 8987, edited by F. H. Teherani, D. C. Look, and D. J. Rogers, International Society for Optics and Photonics (SPIE, 2014) p. 89870K.